

# Optical Engineering

OpticalEngineering.SPIEDigitalLibrary.org

## **Review of three-dimensional imaging of dynamic objects by parallel phase-shifting digital holography**

Takahito Fukuda  
Yasuhiro Awatsuji  
Peng Xia  
Takashi Kakue  
Kenzo Nishio  
Osamu Matoba

**SPIE.**

Takahito Fukuda, Yasuhiro Awatsuji, Peng Xia, Takashi Kakue, Kenzo Nishio, Osamu Matoba, "Review of three-dimensional imaging of dynamic objects by parallel phase-shifting digital holography," *Opt. Eng.* **57**(6), 061613 (2018), doi: 10.1117/1.OE.57.6.061613.

# Review of three-dimensional imaging of dynamic objects by parallel phase-shifting digital holography

Takahito Fukuda,<sup>a</sup> Yasuhiro Awatsuji,<sup>b,\*</sup> Peng Xia,<sup>c</sup> Takashi Kakue,<sup>d</sup> Kenzo Nishio,<sup>e</sup> and Osamu Matoba<sup>f</sup>

<sup>a</sup>Kyoto Institute of Technology, Graduate School of Science and Technology, Department of Electronics, Kyoto, Japan

<sup>b</sup>Kyoto Institute of Technology, Faculty of Electrical Engineering and Electronics, Kyoto, Japan

<sup>c</sup>National Institute of Advanced Industrial Science and Technology, National Metrology Institute of Japan, Research Institute for Measurement and Analytical Instrumentation, Tsukuba, Japan

<sup>d</sup>Chiba University, Graduate School of Engineering, Chiba, Japan

<sup>e</sup>Kyoto Institute of Technology, Advanced Technology Center, Kyoto, Japan

<sup>f</sup>Kobe University, Graduate School of System Informatics, Department of Systems Science, Kobe, Japan

**Abstract.** Parallel phase-shifting digital holography is a powerful technique for recording motion picture of holograms with an image sensor and numerically reconstructing the motion picture of the high-quality three-dimensional (3-D) images of the object in a computer. This technique provides high-quality images of light intensity and phase of the object at a time instant at arbitrary depth position. Therefore, the technique achieves 3-D motion-picture imaging of a dynamic object. The technique provides not only large depth of field and high temporal resolution at the same time but also a motion picture of an invisible object. It is difficult for other 3-D imaging techniques to achieve these features of parallel phase-shifting digital holography. The authors review two experiments demonstrating the 3-D imaging by the technique and the features of the technique. One experiment demonstrated the motion-picture 3-D imaging of a minute crystal, sinking down in solution, by refocusing the amplitude images of the crystal. The result was obtained for the first time, to the best of our knowledge. The other demonstrated the motion-picture 3-D imaging of refractive indices of dynamic invisible gas flow by applying the Abel inversion to the phase images of the flow obtained by the technique. © 2018 Society of Photo-Optical Instrumentation Engineers (SPIE) [DOI: 10.1117/1.OE.57.6.061613]

Keywords: holography, digital holography; 3-D imaging; interferometry; quantitative phase imaging; high-speed imaging.

Paper 171666SS received Oct. 22, 2017; accepted for publication Mar. 16, 2018; published online Apr. 6, 2018.

## 1 Introduction

In recent decades, three-dimensional (3-D) imaging technique has been studied in many fields, such as bioimaging,<sup>1–8</sup> particle measurement,<sup>9–13</sup> flow measurement,<sup>14–19</sup> shape measurement,<sup>20</sup> deformation measurement,<sup>21–25</sup> and so on. Many 3-D imaging techniques such as stereoscopic imaging<sup>26</sup> and light-field imaging<sup>27</sup> have been studied. Especially, holography<sup>28</sup> is an attractive 3-D imaging technique, because the technique obtains not only the light intensity but also the phase information of the object. This is because holography can record the wavefront of a light wave from an object. In this technique, the interference fringe image generated by two light waves is recorded on a holographic plate. One wave is reflected by or transmitted through an object, and the other wave is incident to the holographic plate without illuminating the object. The former and the latter are called as the object wave and the reference wave, respectively. The holographic plate on which the interference fringe image was recorded is called the hologram. When the plate is illuminated by the light wave having the same wavelength and incident angle as the reference wave, the object wave is reconstructed and the 3-D image of the object can be observed. Although holography provides a high-quality 3-D image of an object, it is difficult for the holographic plate to record a motion picture of a hologram. This is because a holographic plate requires a burdensome

process such as the chemical development of the holographic plate after recording the holograms, in general. To avoid the burden, digital holography has been studied.<sup>29</sup> Digital holography records an interference fringe image as digital data using an image sensor such as a charge-coupled device or complementary metal-oxide semiconductor image sensor, instead of a holographic plate. Digital holography reconstructs the amplitude and phase of an object by numerical process and displays the 3-D image in a computer. In particular, parallel phase-shifting digital holography was expected to obtain high-quality 3-D motion-picture of an object.<sup>30</sup> Owing to the capability, many papers have reported high-speed motion-picture 3-D measurement of dynamic biological specimen, invisible air flow, sound-field, wavefront from an optical device, vibration of a loudspeaker, light propagation, and so on.<sup>31–37</sup>

### 1.1 Digital Holography

Because the amplitude and phase distributions of the object wave at arbitrary depth position can be calculated, digital holography can numerically reconstruct the 3-D image of the object. Owing to the acquisition capability of quantitative complex amplitude of the light wave from an object, the technique has been actively studied for 3-D shape measurement, 3-D motion measurement, phase measurement, and so on. However, an image sensor is not able to record the same

\*Address all correspondence to: Yasuhiro Awatsuji, E-mail: [awatsuji@kit.ac.jp](mailto:awatsuji@kit.ac.jp)

interference fringes as a holographic plate completely, because the pixel pitch of the image sensor is too large to resolve fine interference fringes. Then, in-line digital holography, in which object wave and reference wave are on-axis, is often used because in-line digital holography enables us to record more information of the interference fringes and covers a larger measurement range and provides higher resolution than off-axis digital holography. However, there is a problem in in-line digital holography: undesired images, the zeroth-order diffraction wave and conjugate image are superimposed on the image of the object. As a result, the quality of the reconstructed image is degraded.

## 1.2 Phase-Shifting Digital Holography

To reconstruct the image free from the undesired images, phase-shifting digital holography was proposed.<sup>38</sup> Phase-shifting digital holography sequentially records multiple holograms with phase-shifting of the reference wave. From the recorded phase-shifted holograms, the complex amplitude free from the undesired images is numerically reconstructed in a computer as the following procedure. Here, we define the complex amplitude distribution of an object wave on an image sensor plane as  $U_o(x, y) = A_o(x, y) \exp[j\phi(x, y)]$ .  $A_o(x, y)$  is the amplitude,  $\phi(x, y)$  is the phase, and  $j$  is an imaginary unit. We assume that the wave propagates along the  $z$  axis. Although four-step phase-shifting digital holography is often employed, parallel phase-shifting digital holography recording fewer phase-shifted holograms has been proposed so as to reconstruct higher-quality image than that of four-step phase-shifting digital holography.<sup>39,40</sup> We now describe two-step phase-shifting digital holography,<sup>41</sup> for example. Two holograms  $I_0(x, y)$ ,  $I_{\pi/2}(x, y)$  with phase difference  $\pi/2$  are recorded and then complex amplitude of the object wave at the image sensor plane is given as

$$U_o(x, y) = \frac{[I_0(x, y) - a(x, y)] + j[I_{\pi/2}(x, y) - a(x, y)]}{2A_r(x, y)}, \quad (1)$$

$$a(x, y) \equiv A_o^2(x, y) + A_r^2(x, y) \\ = \frac{v(x, y) - \sqrt{v^2(x, y) - 2w(x, y)}}{2}, \quad (2)$$

$$v(x, y) \equiv [I_0(x, y) + I_{\pi/2}(x, y)] + 2A_r^2(x, y), \quad (3)$$

$$w(x, y) \equiv [I_0^2(x, y) + I_{\pi/2}^2(x, y)] + 4A_r^4(x, y), \quad (4)$$

where  $A_r^2(x, y)$  is the intensity distribution of the reference wave.  $U_o(x, y)$ , the complex amplitude distribution of the object wave at the image sensor plane  $z = 0$ , is given by Eq. (1). Then,  $U(x, y, z)$ , the complex amplitude distribution of the object wave at arbitrary depth  $z$ , is obtained by calculating the light propagation in the depth direction. Light propagation can be calculated by several methods such as the Fresnel transformation or the angular spectrum method.<sup>42</sup> Here, we describe the angular spectrum method as follows:

$$U(x, y, z) = \text{FT}^{-1}\{\text{FT}[U_o(x, y)] \exp[-jz(k^2 - k_x^2 - k_y^2)]\}, \quad (5)$$

where  $k = 2\pi/\lambda$ ,  $\lambda$ ,  $k_x$ , and  $k_y$  are the wave number, the wavelength, and the wave numbers in the  $x$  and  $y$  directions, respectively. FT and FT<sup>-1</sup> are the Fourier transform operation and the inverse Fourier transform operation, respectively.

Indeed, phase-shifting digital holography can provide high-quality 3-D imaging of an object free from the undesired images. However, the technique requires sequential recording of multiple holograms. Therefore, the technique is useless for a dynamic object, much less recording motion picture of holograms of the dynamic object. To cope with a dynamic object, parallel phase-shifting digital holography was proposed.

## 1.3 Parallel Phase-Shifting Digital Holography

Parallel phase-shifting digital holography is a technique that implements phase-shifting digital holography with a single-shot recording of multiple phase-shifted holograms, which are required for phase-shifting digital holography, using a single image sensor. Figure 1 shows a schematic of the principle of parallel phase-shifting digital holography. This figure shows the example where the number of the steps of the phase-shifting is  $N$ . In this technique, an image sensor records multiple phase-shifted holograms as a single hologram. The holograms are recorded by each pixel of the sensor based on a space-division multiplexing technique. Two methods have been proposed to derive the complex amplitude of the object. One method interpolates the blanked pixels of each hologram<sup>30</sup> and the other conducts the calculation used in the phase-shifting interferometry using neighboring pixels.<sup>43,44</sup> In this paper, we describe the interpolation method often used. Pixels of each phase-shifted hologram are extracted from the recorded single hologram. Each blanked pixels of each of the phase-shifted holograms is interpolated using the neighboring pixels. After the interpolation, the multiple holograms required for phase-shifting digital holography are generated. Then, the complex amplitude at the image sensor plane is obtained by the calculation used in the phase-shifting interferometry, and the complex amplitude of the object wave at arbitrary depth is obtained by calculation of light propagation.

Owing to the capability of simultaneous recording of multiple holograms, parallel phase-shifting digital holography can record motion-picture 3-D images at the same frame rate as that of the image sensor. In other 3-D imaging techniques, there are trade-off relations between depth of field and temporal resolution or between depth resolution and lateral resolution. In contrast, there are not the relations in parallel phase-shifting digital holography. Furthermore, the technique can obtain a motion picture of an invisible object, because the technique can obtain motion picture of the phase distribution of the object. Both of these are the advantageous features of parallel phase-shifting digital holography compared with other 3-D imaging techniques.

In this paper, we review two experimental demonstrations of the motion-picture 3-D imaging of dynamic objects using parallel phase-shifting digital holography in detail. One used the amplitude distribution and the other used the phase distribution. These distributions of dynamic objects were

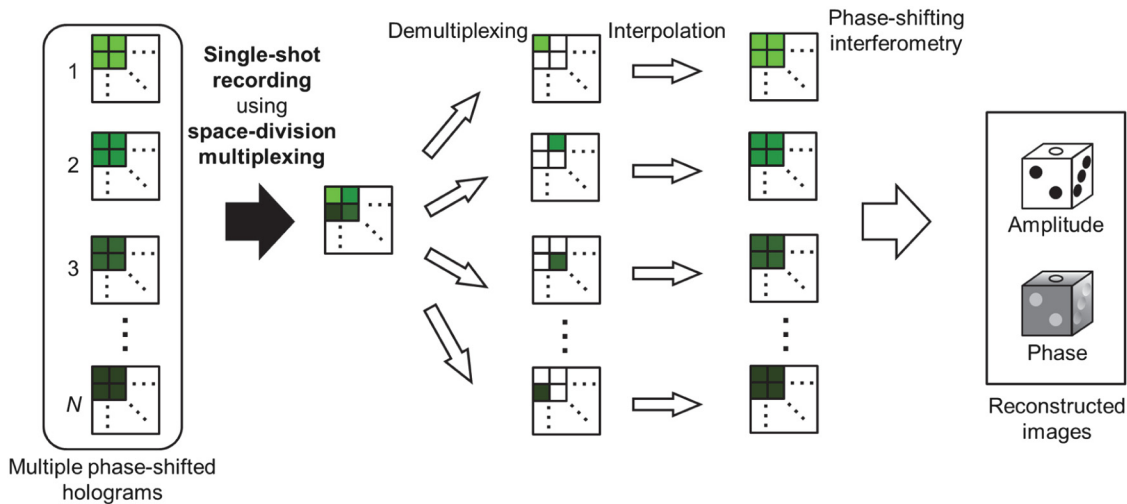


**Fig. 1** Schematic of the principle of parallel phase-shifting digital holography in which the number of the steps of the phase-shifting is  $N$ .

obtained by the technique. Both demonstrations show the features of the technique.

## 2 Three-Dimensional Imaging of a Dynamic Object by Parallel Phase-Shifting Digital Holography

### 2.1 Using the Amplitude Image

In general, the depth of field is quite small in microscopic measurement. Then, we experimentally demonstrated 3-D measurement of a dynamic minute specimen using the amplitude obtained by parallel phase-shifting digital holography and display the measurement result in 3-D space.<sup>45</sup>

#### 2.1.1 Methods

Figure 2 shows the schematic of the optical setup of the experimental system. To implement the parallel phase-shifting, a microphase-shifting array,<sup>30,39,40,43,46</sup> a spatial light modulator,<sup>47</sup> and a microarray device such as a microwave

plate array or a micropolarizer array<sup>31,32,36,37,48–56</sup> have been proposed. This system is a microscope system based on the implementation of parallel phase-shifting digital holography using polarization.<sup>48,56</sup> A light wave is split into two waves by the polarizing beam splitter. The polarization state of the two waves is orthogonal to each other. One wave transmits through a specimen and becomes the object wave, then this wave is combined with the other wave, the reference wave. The half-wave plate is used to adjust the intensity ratio of the two waves adequately. By passing through the quarter-wave plate in front of the camera, the two waves are transformed into clockwise and counterclockwise circularly polarized light waves, respectively. The camera has a micropolarizer array device consisting of the blocks consisting of  $2 \times 2$  cells of micropolarizer, as shown in Fig. 2. Intensities of four linearly polarized light beams are detected by each  $2 \times 2$  pixels of the image sensor after passing through the array device, whose polarization directions are 0 deg, 45 deg, 90 deg, and 135 deg. Therefore, the polarization-imaging

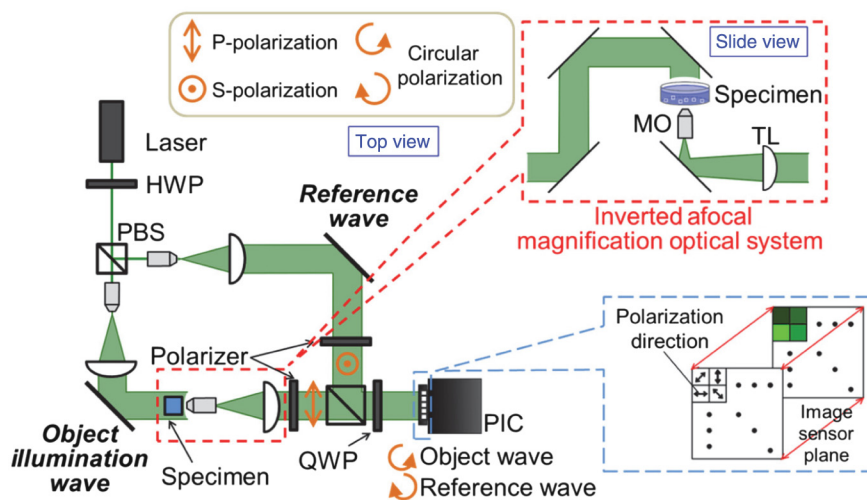


**Fig. 2** Schematic of the optical setup of the microscope system based on parallel phase-shifting digital holography. PBS, polarizing beam splitter; HWP, half-wave plate; QWP, quarter-wave plate; PIC, polarization-imaging camera; MO, microscope objective; TL, tube lens.

camera is capable of capturing two-dimensional (2-D) distribution of polarization state of an incident light into the image sensor. Thus, four interference fringe images with phase differences  $0$ ,  $\pi/2$ ,  $\pi$ , and  $3\pi/2$  are recorded by each of the  $2 \times 2$  pixels of the camera. Consequently, four phase-shifted holograms required for four-step phase-shifting digital holography are recorded by space-division multiplexing technique with a single-shot exposure. We reconstructed the complex amplitude distribution of the object by applying the image-reconstruction algorithm of two-step parallel phase-shifting digital holography to the recorded four holograms.<sup>49</sup>

We set a magnification optical system to measure a minute specimen, and employed an afocal system as the magnification optical system. The afocal system consists of two lenses with the focal lengths of  $f_1$  and  $f_2$ . The lenses are separated by a distance of  $f_1 + f_2$ . The lateral magnification  $M_{\text{lat}}$  and the longitudinal magnification  $M_{\text{long}}$  depend only on both the focal lengths and given as

$$M_{\text{lat}} = f_2/f_1, \quad (6)$$

$$M_{\text{long}} = (f_2/f_1)^2. \quad (7)$$

The longitudinal magnification  $M_{\text{long}}$  is equal to the square of the lateral magnification  $M_{\text{lat}}$ , as shown in Eqs. (6) and (7). Therefore, when the microscope system consists of a microscope objective with a short focal length and a tube lens with a longer focal length, the depth of field is quite small. Consequently, it is difficult for a usual microscope to observe a specimen moving in the depth direction. In contrast, parallel phase-shifting digital holography is capable of motion-picture measurement of a dynamic specimen moving in 3-D, owing to the capabilities of the single-shot recording of holograms and digital refocusing at arbitrary depth. Indeed also light-field imaging achieves 3-D imaging with an image sensor and with a single-shot exposure, but there is a trade-off relation between lateral resolution and depth resolution and this technique cannot obtain the phase image of an object. In contrast, there is not the relation in parallel phase-shifting digital holography and the technique can obtain the phase image.

Furthermore, we employed an inverted system as the magnification optical system, whose specimen is illuminated

from above. This is because an inverted system is suitable for demonstrating motion-picture 3-D imaging of a minute object sinking down in an aqueous solution in the depth direction.

### 2.1.2 Experimental setup

As shown in the dashed line in Fig. 2, the inverted afocal magnification optical system was constructed. The light wave for illuminating the specimen is reflected upward then horizontally by mirrors. The wave is reflected downward by another mirror and directed on a specimen. The wave transmits the specimen and becomes the object wave. After that, the object wave is finally reflected horizontally by the other mirror and recorded by a polarization-imaging camera.

Figure 3 shows the photograph of the optical system shown in Fig. 2. A Nd:YVO<sub>4</sub> laser operated at 532 nm was used as the light source. A Photron FASTCAM-SA2-P whose pixel pitch is 10  $\mu\text{m}$  was used as the polarization-imaging camera. This high-speed camera can record motion picture at the frame rate up to 86.2 kilo frames per second (fps). The inverted afocal magnification optical system consisted of a microscope objective with 16.6-mm focal length and a convex lens with 300 mm focal length. Equations (6) and (7) give the lateral and longitudinal magnifications 18.1 and 328. We use the criterion of resolution defined by Abbe, which is used when specimens are illuminated by a coherent parallel light wave.<sup>57</sup> Then, the lateral resolution  $\delta = \lambda/\text{NA}$  is calculated and 2.1  $\mu\text{m}$  is obtained.

### 2.1.3 Results

First, we recorded salt crystals of 10  $\mu\text{m}$  order precipitated at the bottom of a container filled with solution of salt, then reconstructed the complex amplitude of the crystal. Figure 4 shows the experimental result. Figures 4(a) and 4(c) show the amplitude image and the phase image reconstructed by parallel-phase-shifting digital holography. Figures 4(b) and 4(d) show the amplitude image and the phase image reconstructed by the in-line digital holography without the phase-shifting, for comparison. In the images reconstructed by the in-line digital holography without phase-shifting, the edges of the crystal are seen double, and the contrast was emphasized undesirably, as shown in Figs. 4(b) and 4(d). This is because

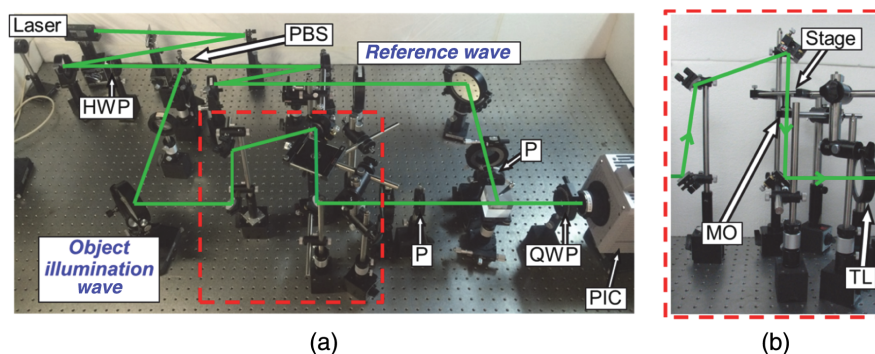


**Fig. 3** Photographs of the constructed optical system of the microscope system based on parallel phase-shifting digital holography. (a) Top view of the whole system and (b) side view of the magnification optical system shown in the dashed line square in (a). PBS, polarizing beam splitter; HWP, half-wave plate; QWP, quarter-wave plate; PIC, polarization-imaging camera; P, polarizer; MO, microscope objective; TL, tube lens.

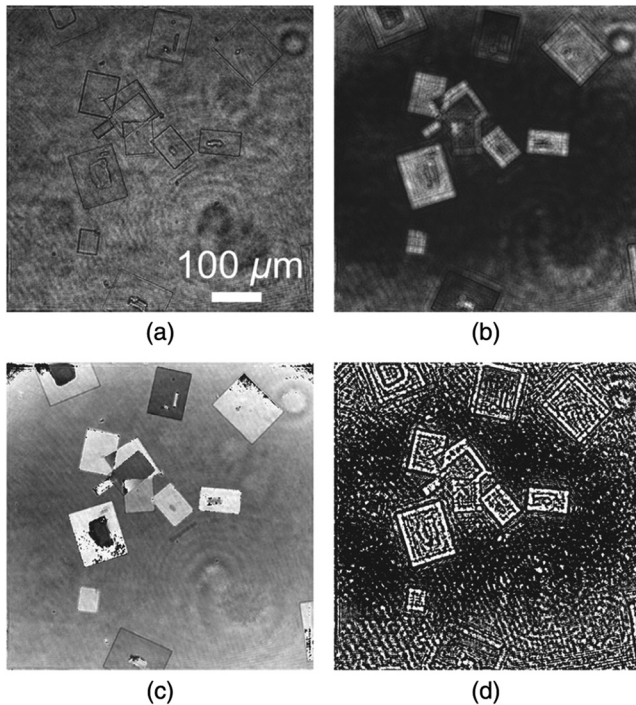


**Fig. 4** Reconstructed images of salt crystals: (a) amplitude and (c) phase images reconstructed by parallel-phase-shifting digital holography, (b) amplitude and (d) phase images reconstructed by the in-line digital holography without phase-shifting.

the undesired images were superimposed on the desired images and interfered with the desired images. In contrast, parallel-phase-shifting digital holography reconstructed clear images free from the unwanted images. Thus, it was demonstrated that parallel phase-shifting digital holography is capable of high-quality imaging of a minute specimen in microscopic measurement.

Next, we recorded an alum crystal sinking down in the solution of alum with the same optical system and displayed

the result in 3-D space. The frame rate, the shutter speed, and the total recording time were 60 fps, 10 ms, and 18 s, respectively. Figures 5 and 6 show the results. Each of the images is the amplitude image extracted from the reconstructed motion picture every 160 frames in Figs. 5 and 6, respectively. Thus, the time interval of the images is 2.67 s. Figure 5 shows the images refocused on the fixed plane where the crystal was located when the recording of the motion picture was finished. The images were not refocused for most of the time on the crystal sinking down in the depth direction, which is the same as the image observed by a usual microscope. Therefore, it is difficult to specify the position and the direction of the crystal. In contrast, Fig. 6 shows the images refocused at all times on the plane where the center of the crystal was. We refocused on a corner of the crystal and defined the depth position when we refocused on the corner as the depth position where the reconstructed image of the corner has the sharpest edge, at each 160 frames. Then, we defined the center of the crystal as the point of an intersection between 3-D diagonal lines of the refocused corners, at each 160 frames. These depth positions were calculated from the propagation distance obtained by calculation of the light propagation of the object wave. The object wave was refracted by the aqueous solution and magnified by the magnification optical system. To calculate the exact position of the crystal, it is necessary to know the refractive index of the aqueous solution and to compensate the refraction. We measured the refractive index of the solution and obtained the value of 1.36. The depth positions  $z$  were calculated from the propagation distance, the refractive index of 1.36, and the longitudinal magnification of 328. These positions are (a) 1020  $\mu\text{m}$ , (b) 997  $\mu\text{m}$ , (c) 871  $\mu\text{m}$ , (d) 655  $\mu\text{m}$ , (e) 334  $\mu\text{m}$ , (f) 87  $\mu\text{m}$ , (g)  $-66 \mu\text{m}$ , and (h)  $-66 \mu\text{m}$ . Here, the  $z$  axis was taken in the counter direction of the direction in which the crystal was sinking down, and  $z = 0$  indicates the depth position where the center of the crystal was located when we started the recording of motion picture of holograms. Figure 6 shows the images refocused at

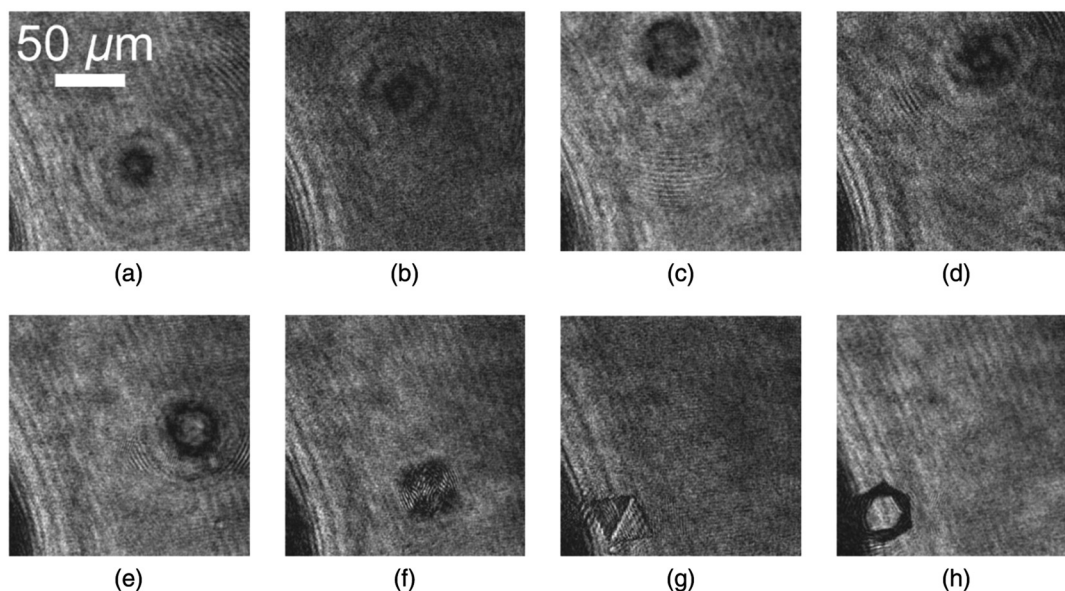


**Fig. 5** Reconstructed amplitude images refocused on the fixed plane. The images were refocused on the plane where the crystal was at (h). Each time interval of (a)–(h) is 2.67 s.

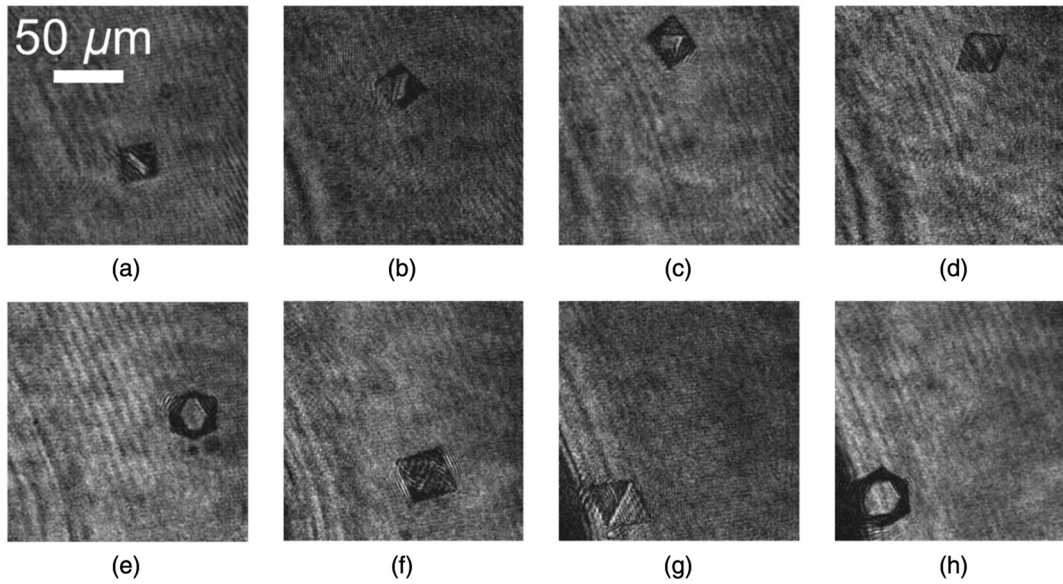


**Fig. 6** Reconstructed amplitude images of minute alum crystal in focus at all time. The crystal was tracked and the images were refocused at all time on the plane where the crystal was. Each time interval of (a)–(h) is 2.67 s. Positions of the crystal in depth direction are  $z =$  (a)  $1020 \mu\text{m}$ , (b)  $997 \mu\text{m}$ , (c)  $871 \mu\text{m}$ , (d)  $655 \mu\text{m}$ , (e)  $334 \mu\text{m}$ , (f)  $87 \mu\text{m}$ , (g)  $-66 \mu\text{m}$ , and (h)  $-66 \mu\text{m}$ .

all time on the crystal sinking down in the depth direction and also shows the crystal was rotating while sinking. As shown in Fig. 6, we successfully demonstrated quantitative 3-D imaging of the crystal, whose shape and size were approximately regular octahedron and about  $25 \mu\text{m}$  in a side, respectively, sinking in the depth direction.

Furthermore, we calculated the 3-D displacement of the crystal. Because the lateral positions were also calculated when the depth positions were calculated, the 3-D positions were found. Figure 7 shows the 3-D trajectory of the crystal. The trajectories in (a) 3-D, (b) the  $x - z$  plane, i.e., top view, (c) the  $y - z$  plane, and (d) the  $x - y$  plane are shown. Each of the open circles shows the position of the center of the crystal at each 20 frames, i.e., each 0.333 s, and the dashed curve shows the trajectory of the center. The  $x - y$  plane shows the lateral plane of the reconstructed image, and the original position shows the lateral position of the crystal when the recording was started. As shown in Fig. 7, we successfully demonstrated quantitative 3-D imaging of the minute crystal sinking in the solution.

## 2.2 Using the Phase Image

In this section, we review the motion-picture 3-D imaging of a dynamic invisible object using the phase image of the object obtained by parallel phase-shifting digital holography.<sup>58</sup>

### 2.2.1 Methods

Because parallel phase-shifting digital holography is capable of instantaneous measurement of the phase distribution of an object with a single-shot exposure, the technique is capable of visualizing and quantitatively measuring an invisible object changing at high speed. However, the phase retrieved by interferometry, including parallel phase-shifting digital holography, expresses only the phase lag caused by a transparent object including an invisible object, in general. Therefore, it is difficult for interferometry alone to measure

the phase variation inside, the shape, nor others of the object, much less imaging a transparent object in 3-D. Then, we applied the Abel inversion to the phase lag distribution retrieved by parallel phase-shifting digital holography and achieved imaging the phase distribution including the inside of the object. Furthermore, we achieved 3-D imaging of the distribution of the refractive index of an invisible object changing at high speed.

A light wave propagating along the  $z$  axis transmits through a transparent object with the refractive index  $n(x, y, z)$ , then the phase lag  $\Delta\varphi(x, y)$  is given as

$$\Delta\varphi(x, y) = \int_{-\infty}^{\infty} \frac{2\pi}{\lambda} \Delta n(x, y, z) dz, \quad (8)$$

where  $\Delta n(x, y, z) = n(x, y, z) - n_0$ ,  $n_0$  is the refractive index of air and  $\lambda$  is the wavelength of the light wave. If the refractive index  $n(x, y, z)$  is axially symmetric about the  $y$  axis, Eq. (8) is rewritten as

$$\Delta\varphi(x, y) = \int_{-\infty}^{\infty} \frac{2\pi}{\lambda} \Delta n(r, y) dz, \quad (9)$$

where the radius  $r = (x^2 + z^2)^{1/2}$ . The relationship between  $\Delta\varphi(x, y)$  and  $(2\pi/\lambda)\Delta n(r, y)$  is called the Abel transform.<sup>59</sup> By operating the Abel inversion or the inverse of the Abel transform of Eq. (9), the radial distribution of the refractive index is calculated as

$$n(r, y) = n_0 + \int_r^{\infty} \frac{\lambda}{2\pi^2} \left[ \frac{d\Delta\varphi(x, y)}{dx} \right] \frac{dx}{\sqrt{x^2 - r^2}}. \quad (10)$$

The 3-D distribution of the refractive index is obtained by rotating the radial distribution around the  $y$  axis.

The 3-D distribution of the refractive index of an object is calculated by substituting the 2-D phase distribution of an object, which is reconstructed by parallel phase-shifting

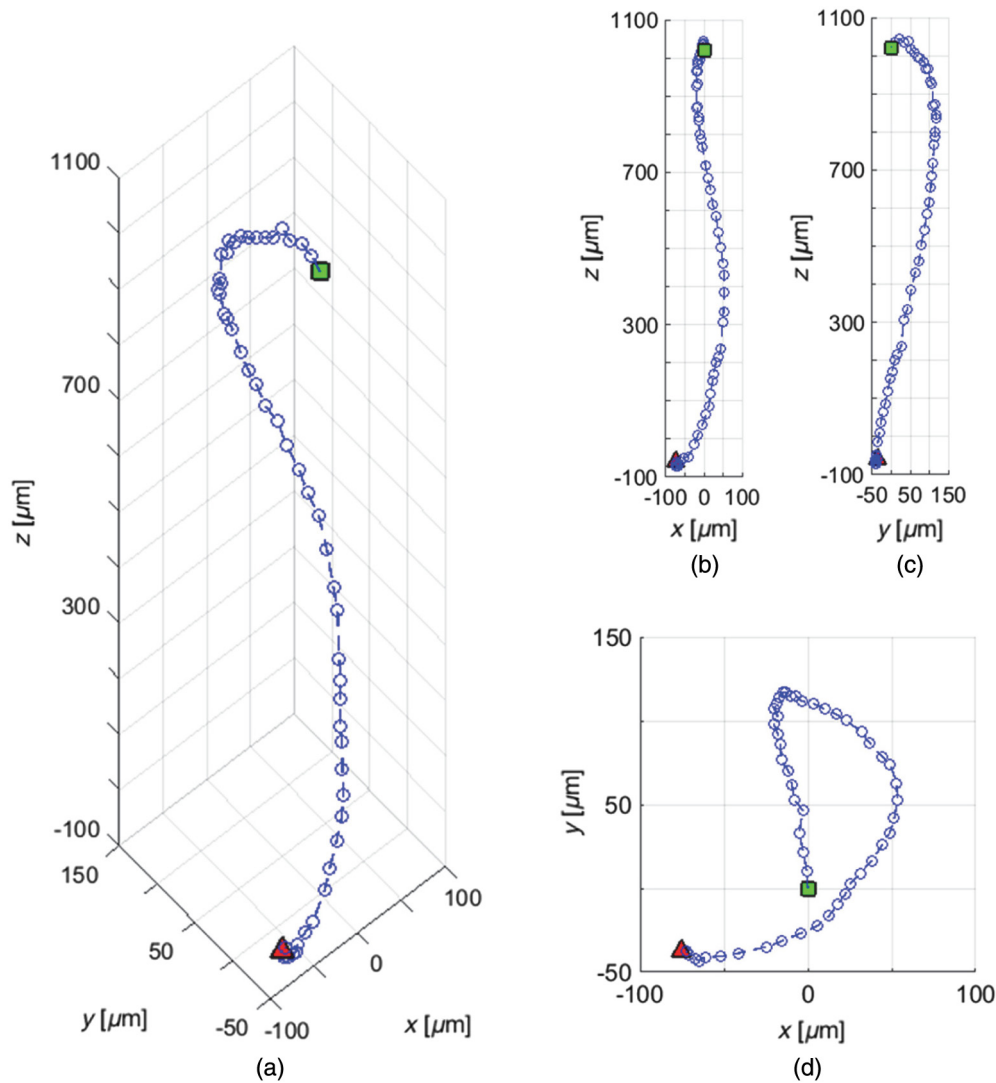


**Fig. 7** 3-D tracking of a minute alum crystal sinking down in aqueous solution. Trajectories in (a) 3-D, (b)  $x - z$  plane, (c)  $y - z$  plane, and (d)  $x - y$  plane. The closed square shows the position when the recording of motion picture of holograms was started, and the closed triangle shows the position when the recording was finished.

digital holography, into the 2-D distribution in Eq. (10). Therefore, motion picture of 3-D distributions of the refractive index of an object changing at high speed is reconstructed. Figure 8 shows the schematic of the flow of the calculation of the motion picture of 3-D distributions. The process is carried out along the following steps:

- (1) We retrieve the 2-D phase distribution  $\varphi(x, y)$  of a light wave transmitted along the  $z$  axis through an object with axially symmetric refractive index with respect to the  $y$  axis.
- (2) The sign of the retrieved phase distribution  $\varphi(x, y)$  is changed and then the phase lag  $\Delta\varphi(x, y)$  is obtained.
- (3) At any  $y$ , the one-dimensional (1-D) phase lag  $\Delta\varphi(x)$  is substituted into  $\Delta\varphi(x)$  in Eq. (10) and the Abel inversion is operated. Then, the radial distribution of the refractive index  $n(r)$  is obtained.
- (4) The 2-D distribution of the refractive index  $n(x, z)$  is obtained by rotating the radial distribution  $n(r)$  around the  $y$  axis.

- (5) At each  $y$ , the steps (3) and (4) are operated.
- (6) Finally, the 3-D distribution of the refractive index  $n(x, y, z)$  of the object is obtained by laminating the 2-D distribution  $n(x, z)$  along the  $y$  axis.

We experimentally demonstrated motion-picture 3-D imaging of the distribution of the refractive index of a dynamic invisible object, by applying the Abel inversion to the phase distribution of the object retrieved by parallel phase-shifting digital holography.<sup>58</sup>

### 2.2.2 Experimental setup

We constructed the optical system of parallel phase-shifting digital holography, which was almost the same system shown in Fig. 2 but without the magnification optical system. We used the same laser and polarization-imaging camera as used in Sec. 2.1. We recorded invisible gas flowed from a nozzle of a commercial gas duster shown in Fig. 9, as an invisible object. The gas consisted of carbon dioxide and dimethyl ether. As shown in Fig. 9, the gas flow is

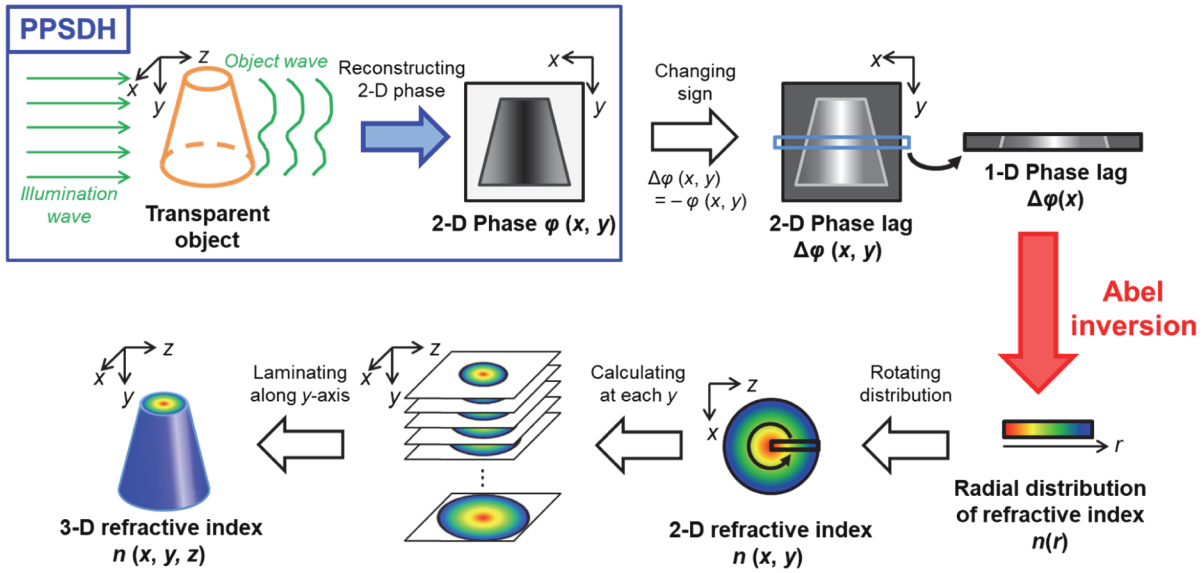


**Fig. 8** Schematic of the calculation flow of the motion picture of 3-D refractive indices of a dynamic transparent object from holograms recorded and phase distributions reconstructed by parallel phase-shifting digital holography.

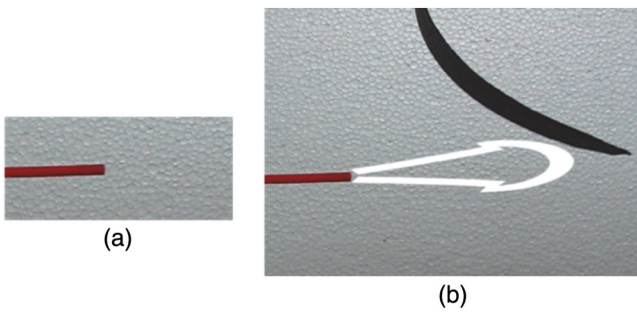


**Fig. 9** Photographs of the gas flow from the nozzle as an invisible dynamic object recorded with a usual camera. (a) Gas flow and the nozzle and (b) gas flow bending a black paper.

invisible to the human eye and the usual camera. The diameter of the nozzle is  $\sim 1$  mm. We recorded motion picture of holograms at the frame rate 3000 fps and the shutter speed  $1/3000$  s. We retrieved the motion picture of the phase with the holograms. The number of the pixels in

the holograms was  $1024 \times 1024$ , and the Abel inversion was applied to  $512 \times 512$  pixels of each of the holograms, respectively.

### 2.2.3 Results

We recorded a motion picture of holograms and retrieved the phase lag images of the gas flow by parallel phase-shifting digital holography. The images extracted from the motion picture are shown in Fig. 10. Figures 10(a)–10(f) show the retrieved phase lag images every five frames, i.e., 2 ms for 10 ms after the gas duster started to blast the gas. Figures 10(g)–10(l) show the retrieved phase lags every 30 frames, i.e., 20 ms for 140 ms after 90 ms after the gas started to be blasted. Each of the phase lags was unwrapped.<sup>60</sup> As shown in Figs. 10(a)–10(f), the movement of the gas that just started to be blasted was visualized. Interestingly, it was found that the periodic phase distributions appeared, as shown in Figs. 10(h)–10(l). As shown in Fig. 10, the 2-D distributions of the phase lag were approximately linearly symmetric about the flow direction.

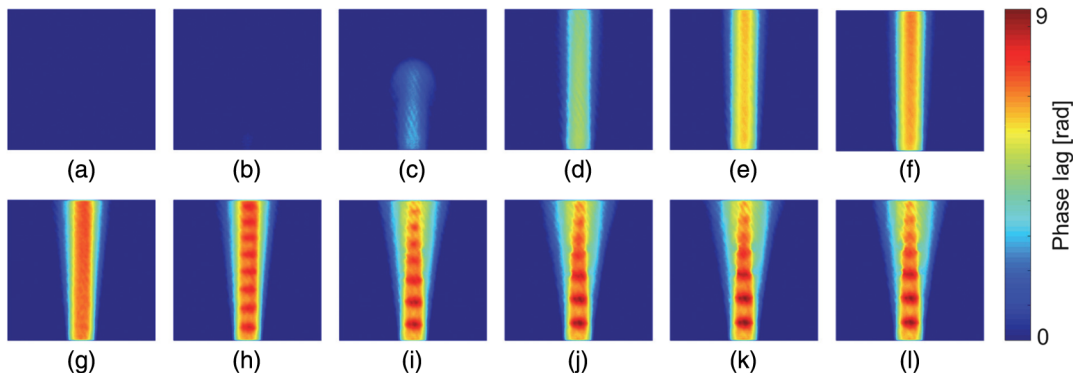


**Fig. 10** Retrieved 2-D phase lag images of the gas flow. Each time interval is (a)–(f) 2 ms, (g)–(l) 10 ms. (a)–(f) After the gas duster started to blast the gas, (g)–(l) after 90 ms after the gas started to be blasted.

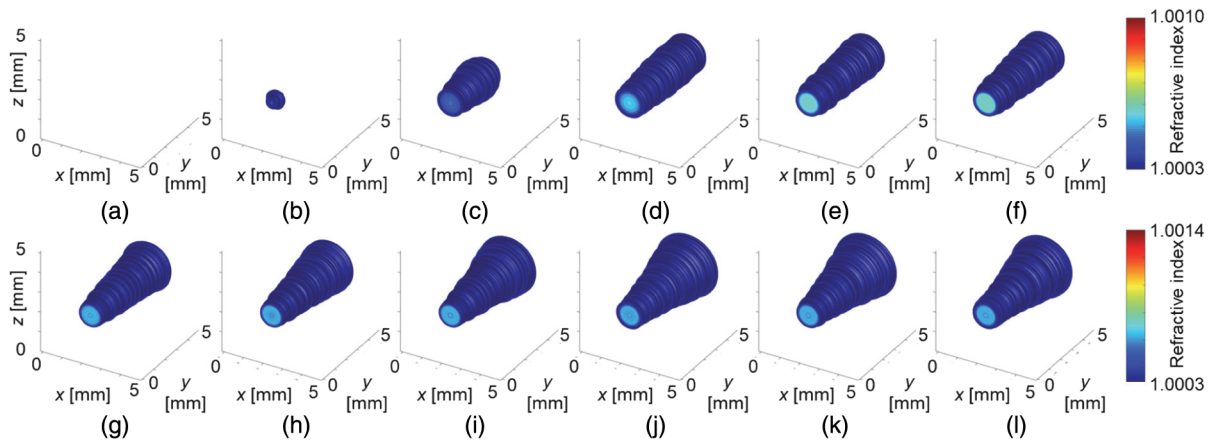


**Fig. 11** Reconstructed 3-D refractive index distributions of the gas flow. Each time interval is (a)–(f) 2 ms, (g)–(l) 10 ms.

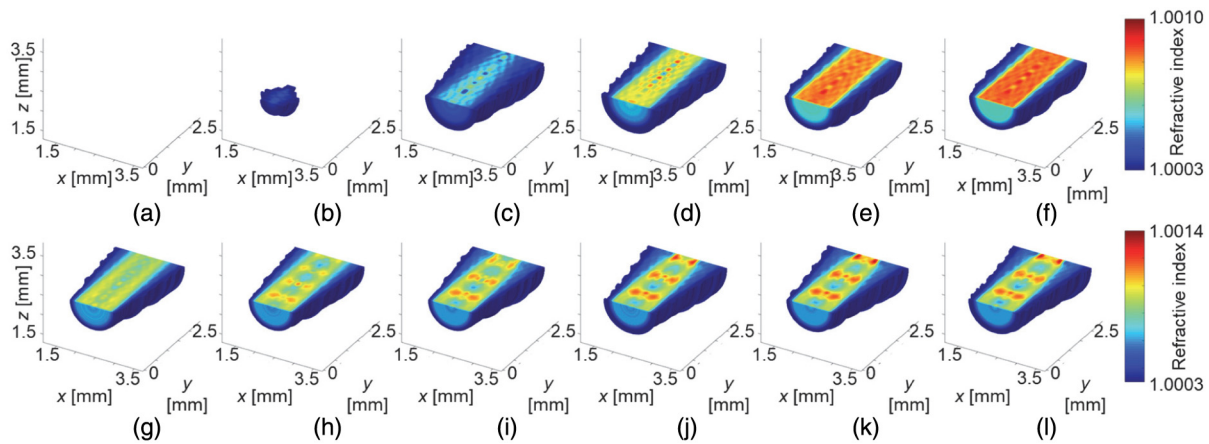


**Fig. 12** Cross-sectional images of the reconstructed 3-D refractive index distributions of the gas flow. The images show one-eighth regions of the 3-D distributions of Fig. 11. Each time interval of is (a)–(f) 2 ms, (g)–(l) 10 ms.

Therefore, we considered that the 3-D distributions of the refractive index were approximately axially symmetric around the flow direction, and then we applied the Abel inversion to the 2-D distributions. Figure 11 shows the calculated 3-D distributions. While the gas flow had a cylindrical shape just after the gas started to be blasted as shown in Figs. 11(a)–11(f), the flow propagated and spread from 90 ms after the gas started to be blasted as shown in Figs. 11(g)–11(l). Although the images show the boundary between the gas and air, the images do not show the distributions inside the boundary. Figure 12 shows the cross-sectional distributions of one-eighth regions of the 3-D distributions of the distributions shown in Fig. 11 having region  $0 \leq x, y, z \text{ (mm)} \leq 5.12$ . Each of the one-eighth regions is  $1.28 \leq x, z \text{ (mm)} \leq 3.86$ ,  $0 \leq y \text{ (mm)} \leq 2.56$ ,  $0 \leq x, y, z \text{ (mm)} \leq 5.12$ . As shown in Figs. 12(g)–12(l), the periodical distributions appeared in the retrieved 3-D distributions of the refractive index, as appeared in the retrieved 2-D distributions of phase lag, from 90 ms after the gas started to be blasted as shown in Fig. 10. Thus, we successfully demonstrated 3-D imaging of the refractive index of the invisible gas flowed at high speed.

### 3 Conclusion

We have reviewed parallel phase-shifting digital holography and the motion-picture 3-D imaging of dynamic objects obtained by parallel phase-shifting digital holography. By using the amplitude image of an object, we demonstrated the 3-D imaging of a minute crystal sinking down in solution in the depth direction. We obtained the motion picture showing the refocused images of the crystal rotating and drawing a spiral. This result was obtained for the first time, to the best of our knowledge. Furthermore, we achieved the 3-D trajectory of the crystal. Also, by using the phase of an object, we demonstrated the motion-picture 3-D imaging of invisible gas flow including the inside of the object. We obtained the motion picture of the 3-D distributions of the refractive index of the gas flow. The 3-D distributions were reconstructed by applying the Abel inversion to the phase distributions retrieved by parallel phase-shifting digital holography.

Parallel phase-shifting digital holography is a powerful technique achieving high-quality 3-D imaging of a dynamic object moving or changing at high speed. This technique can provide not only large depth of field and high temporal resolution but also high spatial resolution, as shown in the

demonstration using the amplitude image. Furthermore, the technique achieves quantitative 3-D imaging of a dynamic, axially symmetric, and invisible object by applying Abel inversion, as shown in the demonstration using the phase image. In future, the technique will achieve motion-picture 3-D imaging of any transparent object including inside of the object by combining with other techniques, even though the object is invisible. Therefore, parallel phase-shifting digital holography will be a very powerful tool in any field of microscopy. The technique will contribute to elucidate the physical mechanism of ultrafast phenomena such as dynamics of plasma, to establish the method to cope with disease, to understand behavior of living cells and cell-cell interaction, and so on.

### Acknowledgments

This study was partially supported by Japan Society for the Promotion of Science (JSPS) KAKENHI Grant-in-Aid for Challenging Exploratory Research.

### References

- S. Tu et al., "Visualizing polymeric bioresorbable scaffolds with three-dimensional image reconstruction using contrast-enhanced micro-computed tomography," *Int. J. Cardiovasc. Imaging* **33**(5), 731–737 (2017).
- J. Rocha et al., "Bacterial type 3 secretion systems: high-throughput 3D single-molecule tracking of sorting platform proteins in live cells," *Biophys. J.* **112**(3), 149a (2017).
- M. Habaza et al., "Rapid 3D refractive-index imaging of live cells in suspension without labeling using dielectrophoretic cell rotation," *Adv. Sci.* **4**(2), 1600205 (2017).
- J. Hur et al., "Melittin-induced alterations in morphology and deformability of human red blood cells using quantitative phase imaging techniques," *Sci. Rep.* **7**(1), 9306 (2017).
- K. A. DiVito et al., "Microfabricated blood vessels undergo neoangiogenesis," *Biomaterials* **138**, 142–152 (2017).
- I. A. Okkelman et al., "Live cell imaging of mouse intestinal organoids reveals heterogeneity in their oxygenation," *Biomaterials* **146**, 86–96 (2017).
- C. Larimer et al., "Design of a dynamic biofilm imaging cell for white-light interferometric microscopy," *Opt. Eng.* **56**(11), 111708 (2017).
- S. Quint et al., "3D tomography of cells in micro-channels," *Appl. Phys. Lett.* **111**(10), 103701 (2017).
- A. K. Rajagopalan et al., "A comprehensive shape analysis pipeline for stereoscopic measurements of particulate populations in suspension," *Powder Technol.* **321**, 479–493 (2017).
- F. H. Kim et al., "Investigation of pore structure in cobalt chrome additively manufactured parts using x-ray computed tomography and three-dimensional image analysis," *Addit. Manuf.* **17**, 23–38 (2017).
- E. M. Hall, D. R. Gueldenbecher, and B. S. Thurrow, "Uncertainty characterization of particle location from refocused plenoptic images," *Opt. Express* **25**(18), 21801–21814 (2017).
- W. Leclerc, "Discrete element method to simulate the elastic behavior of 3D heterogeneous continuous media," *Int. J. Solids Struct.* **121**, 86–102 (2017).
- S. Aghayee et al., "Particle tracking facilitates real time capable motion correction in 2D or 3D two-photon imaging of neuronal activity," *Front. Neural Circuits* **11**, 56 (2017).
- F. Scardulla et al., "Particle image velocimetry study of the celiac trunk hemodynamic induced by continuous-flow left ventricular assist device," *Med. Eng. Phys.* **47**, 47–54 (2017).
- H. Zhang et al., "UmUTracker: a versatile MATLAB program for automated particle tracking of 2D light microscopy or 3D digital holography data," *Comput. Phys. Commun.* **219**, 390–399 (2017).
- F. Huhn et al., "Large-scale volumetric flow measurement in a pure thermal plume by dense tracking of helium-filled soap bubbles," *Exp. Fluids* **58**(9), 116 (2017).
- A. Scanziani et al., "Automatic method for estimation of in situ effective contact angle from x-ray micro tomography images of two-phase flow in porous media," *J. Colloid Interface Sci.* **496**, 51–59 (2017).
- M. Sylwestzak et al., "Massively parallel data processing for quantitative total flow imaging with optical coherence microscopy and tomography," *Comput. Phys. Commun.* **217**, 128–137 (2017).
- X.-B. Li et al., "Measurement of viscoelastic fluid flow in the curved microchannel using digital holographic microscope and polarized camera," *J. Fluids Eng.* **138**(9), 091401 (2016).
- T. Tao et al., "High-precision real-time 3D shape measurement using a bi-frequency scheme and multi-view system," *Appl. Opt.* **56**(13), 3646–3653 (2017).
- D. Wu and H. Xie, "A novel 3D deformation measurement method under optical microscope for micro-scale bulge-test," *Opt. Lasers Eng.* **98**, 190–197 (2017).
- D. Kytýř et al., "Deformation analysis of gellan-gum based bone scaffold using on-the-fly tomography," *Mater. Des.* **134**, 400–417 (2017).
- H. Tang, H. Dong, and Z. Liu, "Study on dynamic deformation synchronized measurement technology of double-layer liquid surfaces," *Opt. Lasers Eng.* **98**, 205–216 (2017).
- X. Guo et al., "Dynamic deformation image de-blurring and image processing for digital imaging correlation measurement," *Opt. Lasers Eng.* **98**, 23–30 (2017).
- S. L. Cann et al., "Characterization of the bone-metal implant interface by digital volume correlation of in-situ loading using neutron tomography," *J. Mech. Behav. Biomed. Mater.* **75**, 271–278 (2017).
- C. Wheatstone, "Contributions to the physiology of vision—Part the first. On some remarkable, and hitherto unobserved, phenomena of binocular vision," *Philos. Trans. R. Soc. London* **128**, 371–394 (1838).
- M. Levoy and P. Hanrahan, "Light field rendering," in *Proc. of the 23rd Annual Conf. on Computer Graphics and Interactive Techniques (SIGGRAPH'96)*, New Orleans, pp. 31–42 (1996).
- D. Gabor, "A new microscopic principle," *Nature* **161**(4098), 777–778 (1948).
- J. W. Goodman and R. W. Lawrence, "Digital image formation from electronically detected holograms," *Appl. Phys. Lett.* **11**(3), 77–79 (1967).
- Y. Awatsuji, M. Sasada, and T. Kubota, "Parallel quasi-phase-shifting digital holography," *Appl. Phys. Lett.* **85**(6), 1069–1071 (2004).
- T. Tahara et al., "High-speed three-dimensional microscope for dynamically moving biological objects based on parallel phase-shifting digital holographic microscopy," *IEEE J. Sel. Top. Quantum Electron.* **18**(4), 1387–1393 (2012).
- T. Kakue et al., "High-speed phase imaging by parallel phase-shifting digital holography," *Opt. Lett.* **36**(21), 4131–4133 (2011).
- K. Ishikawa et al., "High-speed imaging of sound using parallel phase-shifting interferometry," *Opt. Express* **24**(12), 12922–12932 (2016).
- Z. Zhang et al., "Real-time phase measurement of optical vortices based on pixelated micropolarizer array," *Opt. Eng.* **23**(16), 20251–20258 (2015).
- T. Kakue et al., "Digital holographic high-speed 3D imaging for the vibrometry of fast-occurring phenomena," *Sci. Rep.* **7**(1), 10413 (2017).
- T. Kakue et al., "Light-in-flight recording by parallel phase-shifting digital holography," *Appl. Phys. Express* **6**(9), 092501 (2013).
- M. Fujii et al., "A4-sized parallel phase-shifting digital holography system," *J. Disp. Technol.* **10**(2), 132–137 (2014).
- I. Yamaguchi and T. Zhang, "Phase-shifting digital holography," *Opt. Lett.* **22**(16), 1268–1270 (1997).
- Y. Awatsuji et al., "Parallel three-step phase-shifting digital holography," *Appl. Opt.* **45**(13), 2995–3002 (2006).
- Y. Awatsuji et al., "Parallel two-step phase-shifting digital holography," *Appl. Opt.* **47**(19), D183–D189 (2008).
- X. F. Meng et al., "Two-step phase-shifting interferometry and its application in image encryption," *Opt. Lett.* **31**(10), 1414–1416 (2006).
- G. Nehmetallah and P. P. Banerjee, "Applications of digital and analog holography in three-dimensional imaging," *Adv. Opt. Photonics* **4**(4), 472–553 (2012).
- Y. Awatsuji et al., "Scheme to improve the reconstructed image in parallel quasi-phase-shifting digital holography," *Appl. Opt.* **45**(5), 968–974 (2006).
- T. Tahara et al., "Comparative evaluation of the image-reconstruction algorithms of single-shot phase-shifting digital holography," *J. Electron. Imaging* **21**(1), 013021 (2012).
- T. Fukuda et al., "Three-dimensional motion-picture imaging of dynamic object by parallel-phase-shifting digital holographic microscopy using an inverted magnification optical system," *Opt. Rev.* **24**(2), 206–211 (2017).
- M. Sasada et al., "Parallel quasi-phase-shifting digital holography that can achieve instantaneous measurement," in *ICO Int. Conf. Optics and Photonics in Technology Frontier*, pp. 187–188 (2004).
- M. Lin et al., "Parallel phase-shifting digital holography with adaptive function using phase-mode spatial light modulator," *Appl. Opt.* **51**(14), 2633–2637 (2012).
- M. Sasada, Y. Awatsuji, and T. Kubota, "Parallel quasi-phase-shifting digital holography implemented by simple optical set up and effective use of image-sensor pixels," in *ICO Int. Conf. Optics and Photonics in Technology Frontier*, pp. 357–358 (2004).
- T. Kakue et al., "Image quality improvement of parallel four-step phase-shifting digital holography by using the algorithm of parallel two-step phase-shifting digital holography," *Opt. Express* **18**(9), 9555–9560 (2010).
- T. Tahara et al., "Experimental demonstration of parallel two-step phase-shifting digital holography," *Opt. Express* **18**(18), 18975–18980 (2010).
- T. Tahara et al., "Parallel two-step phase-shifting digital holography using polarization," *Opt. Rev.* **17**(3), 108–113 (2010).
- T. Tahara et al., "Parallel phase shifting digital holographic microscopy," *Biomed. Opt. Express* **1**(2), 610–616 (2010).

53. T. Kakue et al., "Single-shot femtosecond-pulsed phase-shifting digital holography," *Opt. Express* **20**(18), 20286–20291 (2012).
54. P. Xia et al., "One million fps digital holography," *Electron. Lett.* **50**(23), 1693–1695 (2014).
55. M. Fujii et al., "Construction of a portable parallel phase-shifting digital holography system," *Opt. Eng.* **50**(9) 091304 (2011).
56. J. E. Millerd et al., "Pixelated phase-mask dynamic interferometer," *Proc. SPIE* **5531**, 304–314 (2004).
57. S. Weisenburger and V. Sandoghdar, "Light microscopy an ongoing contemporary revolution," *Contemp. Phys.* **56**(2), 123–143 (2015).
58. T. Fukuda et al., "Three-dimensional imaging of distribution of refractive index by parallel phase-shifting digital holography using Abel inversion," *Opt. Express* **25**(15), 18066–18071 (2017).
59. K. Bockasten, "Transformation of observed radiances into radial distribution of the emission of a plasma," *J. Opt. Soc. Am.* **51**(9), 943–947 (1961).
60. R. M. Goldstein, H. A. Zebker, and C. L. Werner, "Satellite radar interferometry: two-dimensional phase unwrapping," *Radio Sci.* **23**(4), 713–720 (1988).

**Takahito Fukuda** received his BE degree in electronics from Kyoto Institute of Technology (KIT), Kyoto, Japan, in 2016. He is currently with the Department of Electronics, KIT. His research interests are holography, 3-D imaging, high-speed phase imaging, and 3-D microscopy. He is a member of the Optical Society of Japan (OSJ).

**Yasuhiro Awatsuji** received his BE, ME, and DE degrees from Osaka University, in 1992, 1994, and 1997, respectively. He was a research associate from 1997 to 2005 and an associate professor from 2005 to 2014 at KIT. He has been a professor at KIT since 2014. His research interests are in the area of information optics with emphasis on holography. He is a member of SPIE, OSA, JSAP, and OSJ.

**Peng Xia** received his BE degree in optical information sciences and technology from the University of JiNan, and received his ME and DE degrees in electronics and information science from KIT, Kyoto, Japan, in 2012 and 2015, respectively. He was a research fellow of Japan Society for the Promotion of Science from 2012 to 2016. He is now a researcher in the AIST, Tsukuba, Japan. His research interests include holography and 3-D imaging.

**Takashi Kakue** is an assistant professor at Chiba University. He received his BE, ME, and DE degrees from KIT in 2006, 2008, and 2012, respectively. His current research interests include holography, 3-D display, 3-D measurement, and high-speed imaging. He is a member of SPIE, OSA, IEEE, the OSJ, and the Institute of Image Information and Television Engineers.

**Kenzo Nishio** received his AE degree in electrical engineering from KIT, Kyoto, Japan, in 1984. He became a technical official of KIT, Kyoto, Japan, in 1999. His research interest is physical education. He is a member of the Japanese Society of Microscopy and the Physics Education Society of Japan.

**Osamu Matoba** received his PhD in applied physics from Osaka University, Osaka, Japan, in 1996. He is now a professor in the Department of Systems Science, graduate school of system informatics, Kobe University. His interests are optical sensing including digital holography and OCT, holographic 3-D display, holographic memory, and artificial control of scattering phenomena. He is a fellow of SPIE.